Cl+HD ($v=1$; $J=1,2$) reaction dynamics: Comparison between theory and experiment

S. A. Kandel, A. J. Alexander, Z. H. Kim, and R. N. Zare
Department of Chemistry, Stanford University, Stanford, California 94305

F. J. Aoiz, L. Bañares, and J. F. Castillo
Departamento de Química Física, Facultad de Química, Universidad Complutense, 28040 Madrid, Spain

V. Sáez Rábanos
Departamento de Química y Bioquímica, Escuela Técnica Superior de Ingenieros de Montes,
Universidad Politécnica de Madrid, 28040 Madrid, Spain

Vibrationally state-resolved differential cross sections (DCS) and product rotational distributions have been measured for the Cl+HD($v=1,J=1$)→HCl(DCl)+D(H) reaction at a mean collision energy of 0.065 eV using a photoinitiated reaction (''photoloc'') technique. The effect of HD reagent rotational alignment in the Cl+HD($v=1,J=2$) reaction has also been investigated. The experimental results have been compared with exact quantum mechanical and quasiclassical trajectory calculations performed on the G3 potential energy surface of Allison *et al.* [J. Phys. Chem. **100**, 13575 (1996)]. The experimental measurements reveal that the products are predominantly backward and sideways scattered for HCl($v'=0$) and HCl($v'=1$), with no forward scattering at the collision energies studied, in quantitative agreement with theoretical predictions. The experimental product rotational distribution for HCl($v'=1$) also shows excellent agreement with quantum-mechanical calculations, but the measured DCl+H to HCl+D branching ratio is near unity, which is at variance with the theoretical calculations that predict about 3 times larger yield of HCl+D at these collision energies. The reactivity shows a marked dependence on the direction of the HD($v=1,J=2$) rotational angular momentum, and experimental measurements of this reagent alignment effect are in good agreement with theoretical predictions. © *2000 American Institute of Physics.* [S0021-9606(00)02002-X]

I. INTRODUCTION

Two important experimental and theoretical benchmarks in reaction dynamics are the H+H$_2$ and F+H$_2$ reactions. In order of increasing complexity, Cl+H$_2$ is the next reaction for which a substantial amount of experimental data exists, reliable potential energy surfaces (PES) based on *ab initio* calculations are available, and several quasiclassical trajectory (QCT) and quantum mechanical (QM) dynamical studies have been performed.[1,2]

The Cl+H$_2$ reaction plays a key role in chemical kinetics and serves as a case study for bimolecular reaction rate theories.[3–5] This reaction is also a prototype for a host of Cl-atom reactions that are important in atmospheric chemistry and photochemical air pollution. Kumaran *et al.*[6] have recently summarized the extensive experimental work on rate constants for the Cl+H$_2$ reaction and its isotopic variants. Until very recently, however, several factors have prevented the experimental determination of total and differential cross sections in molecular beam experiments.[7,8] Casavecchia and co-workers[7,8] have measured angular distributions and time-of-flight spectra for HCl at different laboratory scattering angles from the Cl+H$_2$($v=0$) reaction at the collision energy $E_{col}=5.85$ kcal mol^{-1} (0.254 eV). The kinematics of the experiment prevented a neat separation of the HCl($v'=0,J'$) states, but, nevertheless, the experimental

results proved to be sensitive to the rotational state distribution of the HCl product. Liu and co-workers[9] have measured the effects of H$_2$ rotational states and Cl spin–orbit states on the Cl+H$_2$($v=0$) excitation function, and additionally report that the vast majority of HCl products are backscattered. State-resolved DCSs, however, have not yet been reported for this system.

From a theoretical point of view, the calculation of an accurate potential energy surface is at least as challenging as the experimental measurements at the molecular scale. In contrast to the benchmark H+H$_2$ and F+H$_2$ reactions, the *ab initio* calculations for Cl+H$_2$ involve many more electrons, with further complications arising from expected interactions between the valence and core electrons and from spin–orbit couplings. After several attempts to construct a reliable PES for this system based on empirical[10,11] and semiempirical[12] approaches, only recently has it been possible to calculate an *ab initio* PES (hereafter G3);[13] this PES has been successful in reproducing rate constants[6] and molecular beam[8] measurements from QM[8,14] and QCT[8,15] dynamical calculations.

Aoiz and Bañares[16] reported QCT calculations for the Cl+HD($v=0,1;J=0,1$) reaction on the G3 PES at 0.2775 eV and 0.65 eV collision energies. In this work, it was found that the differential cross section (DCS) changes dramatically with vibrational excitation of the reagents. Whereas the

J. Chem. Phys., Vol. 112, No. 2, 8 January 2000

Cl+HD (v=1; J=1,2) reaction dynamics   671

DCS is purely backward for HD(v=0), it becomes strongly forward peaked for reaction with HD(v=1). Furthermore, the forward scattering is state specific, corresponding to HCl product molecules scattered into v'=1. It is interesting that this behavior is qualitatively the same as that experimentally observed for the Cl+CH$_4$(ν_3=1)$\rightarrow$HCl(v'=0,1;J')+CH$_3$ reaction studied by Zare and co-workers using the photoloc/core-extraction technique.[17,18]

The present study of the Cl+HD (v=1; J=1,2) reaction provides the first experimental data on product internal state and scattering distributions and isotopic branching ratios, at a mean collision energy of 0.065 eV. The measurements have been extensively compared with QM and QCT dynamical calculations performed on the G3 PES. In addition, this work presents measurements and calculations of the effect of the alignment of the HD reagent angular momentum on chemical reactivity. The high level of detail available in this study provides an excellent testing ground for the H$_2$Cl PES and for the experimental and theoretical methods employed. This is of particular interest as a new global PES is expected soon to become available for this system,[19] and the comparison between experiment and theory will be an important test for the new surface.

The paper is organized as follows: Sections II and III present the experimental and theoretical methodologies, Sec. IV contains the experimental and theoretical results and the comparison between them, and Sec. V summarizes the main conclusions.

II. EXPERIMENTAL METHODS

In this section a concise summary of the experimental apparatus and techniques pertinent to the present study of the Cl+HD(v=1) reaction is presented, and the reader is referred to previous publications for a more detailed description.[17,18] Briefly, Cl$_2$, HD (Cambridge Isotope, 97% isotopic purity), and helium are premixed in a 1:4:5 ratio and expanded through a pulsed valve into vacuum. The reaction is initiated by production of chlorine atoms from Cl$_2$ photolysis at around 300 nm and by vibrational excitation of the HD reagent using stimulated Raman pumping (SRP). Products are probed after 30–50 ns using 2+1 resonance-enhanced multiphoton ionization (REMPI) through the 2s ←1s transition at 243.1 nm for H and D atom products and through the E←X transition at 247.2 nm for HCl products.[20] Product ions are collected using a velocity-sensitive time-of-flight (TOF) mass spectrometer. It is well established that speed distributions can be used to determine angular scattering (DCSs) of the products from photoinitiated reactions.[21,22] The core extraction technique[17] has been employed to measure product speed distributions, and thus to determine the DCSs for the reaction; more details on the analysis procedure will be presented in Sec. IV A.

An injection-seeded Nd^{3+}:YAG laser (Continuum Powerlite 9020) is used to produce the light necessary for stimulated Raman excitation of the HD reagent into its first vibrational state. In many experiments in other laboratories,[23,24] SRP is effected through the use of the Nd^{3+}:YAG second harmonic (532 nm) and a dye laser to produce tunable red

light. However, we have found that at the fluences necessary for significant population of the HD molecules in v=1, the 532-nm laser light excites the Cl$_2$ precursor electronically, which resulted in large ion backgrounds that renders the experiment untenable. In order to avoid these background signals, the near-infrared output of a dye laser (Continuum ND6000, LDS 751 or LDS 765 dye) is used along with the residual Nd^{3+}:YAG fundamental (1064 nm); these two laser beams are referred to hereafter as the pump and Stokes beam, respectively. Q-branch transitions are at λ_{pump} =767 nm, and the $S(0)$ transition is at λ_{pump}=751 nm. The 1064 nm light is linearly polarized using a thin-film polarizer (CVI Laser Corp., TFP-1064), and a delay line is used to overlap the Nd^{3+}:YAG and dye laser beams temporally. A photoelastic modulator is employed to control the polarization of the dye laser output. The pump and Stokes lasers are combined on a 720–780 nm high reflector at 45° incidence and focused into the reaction chamber using a 300 mm fused silica lens. In order to match the two wavelengths to a HD vibrational transition, a separate cell containing ~1 Torr HD is used, and the resulting coherent anti-Stokes Raman (CARS) signal at ~600 nm is monitored. After optimizing the CARS signal, it is usually possible to adjust the wavelength and spatial overlap in the molecular beam by observing reaction product signals. Typical laser powers are 400 mJ/pulse for the Stokes beam, and 50–70 mJ/pulse for the pump beam; laser bandwidths are approximately 0.003 cm^{-1} and 0.1 cm^{-1}, respectively.

The polarization of the pump beam is controlled on an every-other-shot basis to be parallel or perpendicular to the Stokes laser polarization. Because Q-branch transitions have large oscillator strengths only when the SRP polarizations are parallel, the population of the HD(v=1) reagent can be controlled by switching between parallel and crossed geometries. A 20-fold enhancement in reactive signal was observed when pumping HD(v=1) $Q(1)$ with parallel as opposed to crossed polarization geometries. No other aspect of the experiment depends on the relative directions of the SRP laser polarizations. Consequently, measurement of differences between parallel and crossed geometries constitutes an extremely effective method for distinguishing reaction products from background signals.

Polarized stimulated Raman excitation on O- and S-branch transitions can be used to create vibrationally excited populations with significant rotational alignment.[25] The effect of reagent alignment on reactivity has been investigated by pumping the $S(0)$ transition with parallel laser polarization to produce HD(v=1,J=2,M=0); that is, the HD rotational axis is always perpendicular (classical limit) to the laser polarization. The $S(0)$ transition has been chosen because it results in the largest HD alignment and because this alignment is determined by two-photon selection rules and not by linestrengths. The HD alignment is therefore independent of laser power, ignoring strong-field (state-mixing) effects. The impact of the prepared alignment on the Cl+HD reactivity is then measured by acquiring data with both the pump and Stokes laser polarization vectors either parallel or perpendicular to the TOF axis. These polarizations are simultaneously rotated by using an achromatic waveplate (CVI

Laser Corp., ACWP 700–1100), which alternates position every 10 s to ensure minimal drift of other experimental parameters. For these reagent alignment experiments, care was taken to ensure that there were no polarization-dependent optics after the waveplate.

The ultraviolet (UV) laser light for Cl_2 photodissociation is produced either at 299 nm or 303 nm by the same Nd^{3+}:YAG laser employed for SRP. At these wavelengths, more than 98% of the Cl atoms produced are in the ground $^2P_{3/2}$ electronic state.[26] Laser light at 299 nm is obtained by Stokes-shifting the fourth harmonic of the Nd^{3+}:YAG laser (266 nm) in a high-pressure hydrogen cell; the residual 532 nm light from the Nd^{3+}:YAG is then used to pump the dye laser to produce the SRP pump beam. Alternatively, 303 nm laser light is obtained by frequency doubling the output of an additional dye laser (Spectra Physics PDL-2) operating on rhodamine 640 dye; in this case, the 532 nm output of the Nd^{3+}:YAG is split to pump both the photolysis dye laser and the SRP pump laser. For either photolysis wavelength, 5–10 mJ/pulse is gently focused to a ~1 mm diameter spot at the interaction region. A half waveplate is used to place the photolysis laser polarization either parallel or perpendicular to the TOF axis.

The D, H, and HCl reaction products were observed and it was verified that each of their signals depended on (1) presence of SRP, photolysis, and probe lasers, (2) SRP and probe lasers being on resonance, (3) SRP pump and Stokes beams having parallel polarizations for Q-branch excitation, and (4) presence of Cl_2 and HD in the reaction mixture. The high sensitivity of the two-photon Lyman-α transition allows facile detection of the D-atom product; virtually no background signals impede measurement. H-atom products are detected, however, with more difficulty, because there are large nonresonant background signals, presumably from photodissociation and ionization of pump oil or other contaminants. These background signals are removed by the subtraction procedure but nonetheless result in a decrease of the signal-to-noise ratio. Detection of HCl was difficult, and the signal-to-noise obtained was sufficient to measure $v'=1$ product rotational distributions but insufficient to acquire TOF profiles. Signal-to-noise considerations did not allow the measurement of DCl products.

In the present experiments, the spread in collision energy resulting from residual thermal motion of HD must be taken into account. The range of collision energies contributing to reaction is particularly large because of the large thermal velocities of the light HD reagent. The reagent mixture was cooled through supersonic expansion; however, molecular expansions containing a large fraction of hydrogen often do not show substantial translational cooling. Additionally, the experiments required a relatively gentle supersonic expansion in order to avoid the production of clusters. An upper bound for the beam translational temperature was obtained experimentally by measuring ion arrival profiles for H_2 under similar expansion conditions as those used in the Cl+HD experiments. H_2 was ionized using 3+1 REMPI at 246 nm; there are many Rydberg states available near this wavelength,[27] and no particular efforts were made to identify the nature of the intermediate state used for this process.
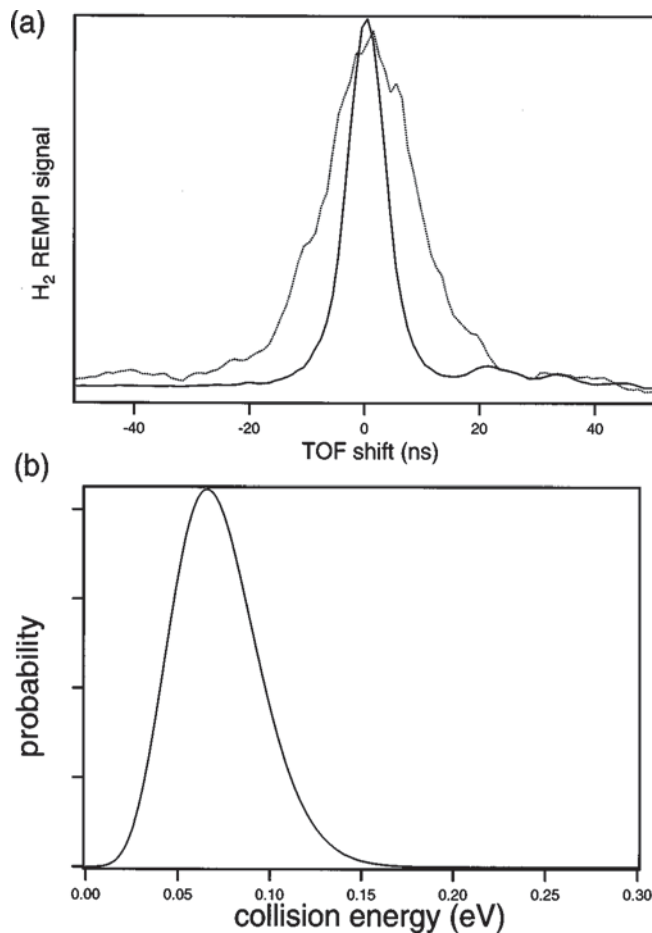

FIG. 1. (a) Measurement of the molecular beam translational temperature. H_2 is ionized using 3+1 REMPI and the resulting ion arrival profile is broadened by thermal motions. A room-temperature sample (dashed line) obtained by back-filling the reaction chamber is compared to H_2 in the molecular beam (solid line). Concentrations in the molecular beam are similar to those used during the experiments. The beam temperature is estimated to be 50 K. (b) Collision energy distribution for the photoinitiated Cl+HD reaction by photodissociation of Cl_2 at 299 nm or 303 nm, assuming a beam temperature of 50 K. The FWHM of the distribution is approximately 0.055 eV.

Figure 1(a) shows the ion arrival profile for H_2^+ in our molecular expansion and compares it to the ion arrival profile for room-temperature H_2, measured via backfilling the chamber. Clearly, the jet expansion results in a significant narrowing of the profile. The instrumental resolution does not permit the measurement of very low translational temperatures, but the present data allow us to establish an upper bound of 50 K. This upper bound has been used to calculate the distribution of center-of-mass collision energies accessed in the current study,[28] which is graphed in Fig. 1(b). The collision energy distribution peaks at 65 meV and is approximately Gaussian in form, with a full-width-at-half-maximum (FWHM) of 55 meV. This spread in collision energy is substantial and needs to be taken into account in both the determination of product scattering and in the comparisons with the theoretical results.

III. THEORETICAL METHODS

All the theoretical calculations have been carried out on the G3 PES.[13] The QM reactive scattering calculations have

been performed for the Cl+HD($v=1,J=1$) reaction using a coupled-channel hyperspherical coordinate method[29,30] at a total energy of 0.7571 eV, which corresponds to the mean collision energy of the experiment ($E_{col}=0.065$ eV). It was found that reaction probabilities were well converged with the parameters used for the present calculations, $E_{max}=2.0$ eV, $J_{max}=16$, and $K_{max}=2$. The use of these parameters results in a coupled-channel basis set containing a total of 287 channels for total angular momentum $J_{tot}=0$. For $J_{tot}\geq 2$ there are 804 channels for HD($v=1,J=1$),$(-1)^{J_{tot}}=-1$, and 517 channels for HD($v=1,J=1$),$(-1)^{J_{tot}}=1$. Calculations up to $J_{tot}=19$ were needed to get converged DCSs.

The general method for the calculation of quasiclassical trajectories is the same as the one used previously (see for instance Ref. 2). In the present work, we have carried out calculations of the collision energy dependence of the reaction cross sections, i.e., the excitation function, $\sigma_R(E_{col})$, for the two channel reactions Cl+HD($v=1,J=1,2$) →HCl(DCl)+D(H). A batch of 500 000 trajectories was run for each of the Cl+HD($v=1,J=1,2$) reactions in the energy interval between the reaction threshold and 0.3 eV. As in previous works, the $\sigma_R(E_{col})$ were subsequently calculated by the method of moments expansion in Legendre polynomials[31,32] using the reduced variable $r=(2E_{col}-E_2-E_1)/(E_2-E_1)$, where E_1 and E_2 are the minimum and maximum collision energies for which the trajectories are run. Using the same batches of trajectories, the collision energy dependence of the vibrationally state-resolved DCSs was obtained by using a double expansion in Legendre polynomials with arguments r and $\cos\theta$ as described in Ref. 2. In addition, batches of 200 000 and 300 000 trajectories were run for Cl+HD($v=1,J=1$) at $E_{col}=0.065$ eV, and for Cl+HD($v=1,J=2$) at $E_{col}=0.1$ eV, respectively. The method of moments expansion in Legendre polynomials was used also to calculate the v' state-resolved DCSs from these batches of trajectories at fixed collision energy.[33]

In all the QCT calculations, the integration step size in the trajectories was chosen to be 5×10^{-17} s, which guarantees a conservation of the total energy better than 1 in 10^5 and better than 1 in 10^7 in the total angular momentum. The initial rovibrational energies of the reagent and product molecules were calculated using the asymptotic diatomic potentials of the PES, and they were fit subsequently to a Dunham expansion in $v+1/2$ and $J(J+1)$. The assignment of product quantum numbers v',J' was carried out by equating the square of the modulus of the classical rotational angular momentum of the HCl(DCl) molecule to $[J'(J'+1)]\hbar^2$. With the (real) J' value so obtained, the vibrational quantum number v' is found by equating the internal energy of the HCl(DCl) molecule to a Dunham expansion. The values of v' and J' found in this way were then rounded to the nearest integer.

As has been addressed elsewhere,[2,34,35] QCT calculations can be exploited not only to get information on scalar properties but also on vector correlations. The $\mathbf{k},\mathbf{J},\mathbf{k}'$ vector correlation can provide useful information about the stereodynamics of chemical reactions and, in particular, the role of the direction of the reagent rotational angular momentum on the reactivity. In what follows, $\mathbf{k}$ and $\mathbf{k}'$ are defined to be the directions of the reagent and product relative velocities, respectively, and $\mathbf{J}$ the direction of the reagent rotational angular momentum. The $\mathbf{k}$ vector is taken to be along the z axis and the xz plane is defined as the one containing $\mathbf{k}$ and $\mathbf{k}'$, such that $y\equiv\mathbf{k}\times\mathbf{k}'$.

From the classical point of view, the most complete information about the $\mathbf{k},\mathbf{J},\mathbf{k}'$ vector correlation is given by the *joint* probability density function, $P(\theta,\theta_J,\phi_J)$, which represents the relative reaction probability into a scattering angle θ, when the $\mathbf{J}$ vector points along a direction defined by θ_J and ϕ_J in the center-of-mass (CM) scattering frame. As in the case of the $\mathbf{k},\mathbf{k}',\mathbf{J}'$ vector correlation, the full spatial distribution of the three $\mathbf{k},\mathbf{J},\mathbf{k}'$ vectors can be expressed as an expansion in modified spherical harmonics.[34–36] The moments of the distribution (the expansion coefficients) can be written as a set of generalized polarization dependent differential cross sections, $S_{kq}(\cos\theta)$, i.e.,

$$P(\theta,\theta_J,\phi_J)=\frac{1}{4\pi}\sum_{kq}(2k+1)S_{kq}(\cos\theta)C_{kq}^*(\theta_J,\phi_J).$$
(1)

The S_{kq} are, in general, imaginary functions. To obtain real J-PDDCSs it is convenient to employ the Hertel–Stoll convention:

$$S_{q+}^{\{k\}}(\cos\theta)=\frac{1}{\sqrt{2}}[(-1)^q S_{k+q}(\cos\theta)+S_{k-q}(\cos\theta)],$$

$$S_{q-}^{\{k\}}(\cos\theta)=\frac{-i}{\sqrt{2}}[(-1)^q S_{k+q}(\cos\theta)-S_{k-q}(\cos\theta)],$$
(2)

$$S_0^{\{k\}}(\cos\theta)=S_{k0}(\cos\theta).$$

Symmetry considerations resulting from the invariance of the distribution of the product internuclear axis upon reflection on the scattering plane constrain the real J-PDDCSs[2,34–36] so that the $S_{q+}^{\{k\}}$ and $S_0^{\{k\}}$ are nonzero only for even k, and the $S_{q-}^{\{k\}}$ are nonzero for odd k.

The θ-independent *J-polarization parameters*, denoted as $s_q^{\{k\}}$, are obtained from the J-PDDCSs by integration over all scattering angles θ. In terms of the expectation values of the multipole moments of $\mathbf{J}$, the first real polarization parameters are

$$s_{1+}^{\{1\}}=\langle\sin\theta_J\sin\phi_J\rangle=\langle J_y/J\rangle,$$

$$s_0^{\{2\}}=\langle P_2(\cos\theta_J)\rangle=\langle(3J_z^2-J^2)/2J^2\rangle,$$

$$s_{1+}^{\{2\}}=\sqrt{3}\langle\sin\theta_J\cos\theta_J\cos\phi_J\rangle=\sqrt{3}\langle J_xJ_z/J^2\rangle,$$

$$s_{2+}^{\{2\}}=\frac{\sqrt{3}}{2}\langle\sin^2\theta_J\cos2\phi_J\rangle=\frac{\sqrt{3}}{2}\langle(J_x^2-J_y^2)/J^2\rangle,$$

where J_x, J_y, and J_z are the components of $\mathbf{J}$ along the x, y, and z axes, respectively. Therefore, each polarization parameter contains information on either the orientation (odd

moments) or the alignment (even moments) of the direction of the initial rotational angular momentum for reactive collisions.

Also of importance are the *renormalized J-PDDCSs*, $S_q^{\{k\}}/S_{00}(\cos \theta)$, which describe the degree of reagent alignment or orientation as a function of θ, with the product flux at each angle normalized out. The renormalized *J-PDDCSs* lend themselves to intuitive physical pictures of the reagent alignment effects. They have the same physical meaning as the polarization parameters, except that they represent the *conditional* expectation values at a given CM scattering angle. In this paper we deal primarily with the $S_0^{\{2\}}/S_{00}$, $S_{1+}^{\{2\}}/S_{00}$, and $S_{2+}^{\{2\}}/S_{00}$ moments.

The $S_0^{\{2\}}/S_{00}$ moment contains information on the sensitivity of the reaction to the *alignment* of initial **J** with respect to **k**. The classical limiting values are $[-1/2, 1]$. The $-1/2$ limit implies that the reaction takes place with reagent molecules whose **J** is perpendicular to **k** (therefore, lying in the *xy* plane). The $+1$ limit implies that reaction prefers reagent molecules whose **J** vector lies along the $z(=\mathbf{k})$ axis.

The $S_{1+}^{\{2\}}/S_{00}$ polarization moment contains information on the preference of reaction for **J** *alignment* along the $x+z$ axis (positive values) or along the $x-z$ axis (negative values); that is, the tilting of **J** with respect to the *xy* and *yz* planes. Its maximum classical value is $+\sqrt{3}/2$ and corresponds to the situation in which **J** is on the $xz(\mathbf{kk}')$ plane along the $x+z$ axis. The zero value might correspond to two different situations: **J** along the *x* or *z* axis or, irrespective of the *x* and *y* components, along the *y* axis; i.e., *xy* and *yz* are nodal planes. The minimum value, $-\sqrt{3}/2$, indicates that reaction prefers to take place when **J** lies along the positive or negative $x-z$ axis.

Finally, the $S_{2+}^{\{2\}}/S_{00}$ polarization moment gauges the relative preference for **J** alignment along the *x* axis with respect to the *y* axis ($=\mathbf{k} \times \mathbf{k}'$). A positive value of this moment implies that product molecules will be preferentially ejected in the plane containing **k** and **J**, whereas a negative value corresponds to the case where product molecules recoil out of the **k**–**J** plane.

IV. RESULTS AND DISCUSSION

A. Experimental results

1. Internal state and velocity distributions

HCl state distributions and H and D atom velocity distributions were measured for the $Cl+HD(v=1, J=1)$ reaction with the HD molecules vibrationally excited via the $Q(1)$ transition using SRP. Note that Q-branch excitation precludes significant reagent alignment. The rotational state distribution of the $HCl(v'=1)$ products was recorded by $2+1$ REMPI using the $(0,1)$ band of the $E \leftarrow X$ transition. The use of the E state as intermediate causes significant dissociation of the detected HCl, resulting in large H^+, Cl^+, and HCl^+ signals. Therefore, the total H^+ intensities from $Q(1)-Q(5)$ transitions were measured, and the $HCl(v'=1)$ rotational populations were calculated using the empirical correction factors reported elsewhere.[18] The resulting rotational distribution, which is shown in Fig. 2, shows significant rotational excitation, peaking at $J'=3$. Additionally, the
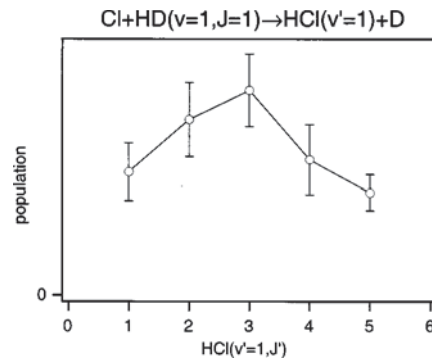

FIG. 2. $HCl(v'=1)$ rotational state distribution for $Cl+HD(v=1, J=1)$ at 0.065 eV mean collision energy. Data are obtained from REMPI spectra of the $E(0,1)$ Q-branch, and populations are determined through the use of empirical correction factors. Error bars are statistical and represent one standard deviation.

total H^+ and D^+ intensities were measured while scanning over the H and D REMPI lines; assuming identical detection efficiencies, a $(DCl+H):(HCl+D)$ branching ratio of $(0.9 \pm 0.2):1$ was obtained.

The ion arrival profile for the D-atom products is shown in Fig. 3(a). The profile was recorded at a photolysis wavelength of 303 nm and with polarization perpendicular to the TOF axis. Measurements of the D-atom profile at 299 nm photolysis in a parallel polarization geometry yielded very similar results. The direction of the SRP pump laser polarization was flipped every other laser shot to distinguish reactive signal from backgrounds, as was detailed in Sec. II. Measurements of the H-atom profile showed reduced signal-to-noise, and additionally, the profile is difficult to analyze; we will discuss the H-atom data only briefly in the Sec. IV C.

The D^+ arrival profile was analyzed to obtain the product speed distribution, which is presented in Fig. 3(b). Because of the low mass of the D atom and the large vibrational spacing of the HCl molecule, the kinematics of the HCl+D product channel are quite favorable for the present study. D-atom products formed in coincidence with $HCl(v'=0)$ have about 2.2 times the center-of-mass velocity than those formed in coincidence with $HCl(v'=1)$. Consequently, the vibrational state of the HCl product can be determined from the D-atom speed distribution. The distribution in Fig. 3(b) is presented with a vertical dashed line which demarcates the possible ranges of D-atom speeds for HCl formed concomitantly with $v'=0$ and $v'=1$; all D-atom speeds slower than 4500 m/s correspond to $HCl(v'=1)$ product molecules, and speeds faster than 4500 m/s correspond to $HCl(v'=0)$.

2. Differential cross sections

The measured D-atom speed distribution shown in Fig. 3(b) was analyzed in order to extract vibrationally state-resolved CM DCSs. The analysis method requires, however, some assumptions about the dependence of reactivity on the HCl rotational state and on the collision energy of the experiment. In order to convert product speeds into scattering angles, we have generated sets of basis functions equally spaced in $\cos \theta$. The HCl rotational distribution was accounted for by generating multiple sets of basis functions
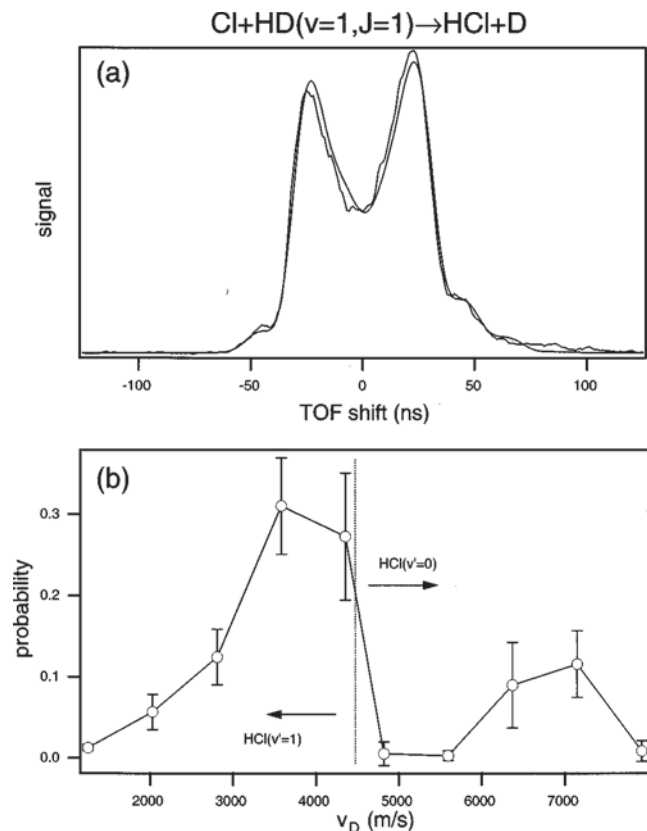
FIG. 3. (a) D^+ arrival profile for Cl+HD($v=1,J=1$) at 0.065 eV mean collision energy. Experimental data are plotted along with the best fit, from which the speed distribution and differential cross sections are obtained. (b) D-atom speed distribution resulting from a best fit to the ion arrival profiles; error bars represent one standard deviation. Due to the favorable kinematics of the reaction, formation of different product HCl vibrational states results in markedly differing D-atom speeds. The speed distributions are plotted along with vertical dashed lines which indicate the range of speeds possible for D atoms formed concomitantly with each possible product vibrational state of the HCl molecule.

FIG. 4. Differential cross sections for HCl($v'=0$) and HCl($v'=1$) products from the Cl+HD($v=1,J=1$) reaction. The scaling of the ordinate axis of both panels reflects the 3.5:1 branching ratio in favor of the vibrationally excited product. Error bars represent one standard deviation.

that assume different product internal energies. These basis functions were then summed together and weighted appropriately according to the theoretical (QM) rotational distribution (the experimental and QM distributions are in excellent agreement; see below). Rotationally state-averaged sets of basis functions for 10 collision energies between 40 meV and 150 meV were then generated and averaged over the collision energy distribution corresponding to a translational temperature of 50 K [shown in Fig. 1(b)], and weighted with the QCT integral cross sections (see below). The resulting basis functions so constructed were then used to fit the D^+ arrival profile in order to obtain the HCl($v'=0$) and HCl($v'=1$) DCSs which are shown in Fig. 4. As there is ambiguity between forward scattered HCl($v'=0$) and backward scattered HCl($v'=1$), the HCl($v'=0$) DCS was fit for $\cos\theta \leqslant 0.4$. The resulting DCSs represent the product scattering averaged over the range of collision energies and summed over the product rotational states. In Fig. 4, the scales of the HCl($v'=0$) and HCl($v'=1$) DCSs are referred to the same relative units; thus by integrating these cross sections over scattering angle, a vibrational state branching ratio of 3.5:1 for HCl($v'=1$):HCl($v'=0$) has been ob-
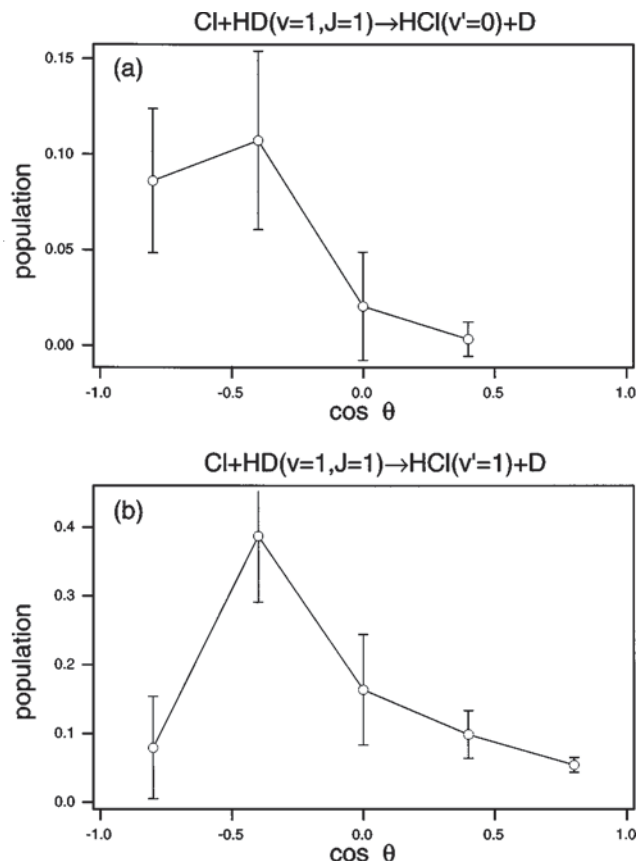
tained. An identical analysis of the data assuming a 100 K beam temperature was performed, obtaining very similar results.

In order to demonstrate the reliability of the analysis method employed to extract the DCS the QCT DCSs as a function of collision energy (see below) were used to simulate an "artificial" ion arrival profile assuming a 50 K translational temperature for the HD molecular beam. We then fit these data and compared the resulting average scattering with the actual (theoretical) collision energy averaged DCSs used as the input for the simulation. In analyzing this artificially constructed data, translational temperatures of 50 K and 100 K were assumed. The resulting fits are comparable to the actual theoretical result. In general terms, the agreement is good, lending credit to the analysis method employed, even with inaccuracies in the estimation of the molecular beam temperature.

Sources of error in the analysis indubitably arise from several assumptions that are made. A 50 K HD translational temperature is assumed; if the actual temperature differs significantly from this value, small changes in the computed DCS would result. In a similar fashion, the analysis is mostly insensitive to the integral cross section, though large deviations in the theoretical values used will result in some error. Next, the analysis assumes that the theoretical HCl($v'=0$) rotational state distribution is correct. However, owing to the
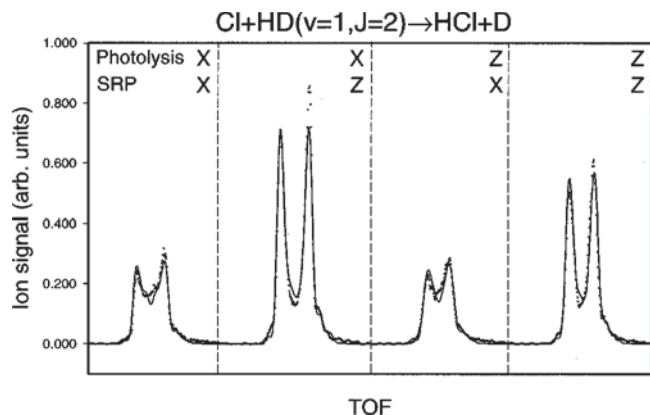
FIG. 5. Dependence of experimental D^+ arrival profiles on photolysis and SRP polarizations. HD($v=1, J=2$) was prepared with a large rotational alignment via $S(0)$ excitation. This alignment causes dramatic changes in signal as a function of pump and photolysis polarization (see text for details). In this experiment, we define the detection axis as Z. The points are the data, the solid line shows the best fit.

large amount of translational energy available in the D+HCl($v'=0$) channel, the exact amount of rotational energy will have little impact on the calculated scattering. Finally, the analysis procedure implicitly assumes that the DCS does not change appreciably with collision energy or with the product rotational state; this assumption is likely to be inexact. Despite errors introduced by assumptions in the analysis, we find that the broad features of the inverted scattering distributions will be correct. Assignment of populations in adjacent bins in the DCS are not as well determined. For example, the HCl($v'=1$) DCS is roughly back scattered with a peak at $\cos\theta=-0.5$, dropping sharply for more backward scattered trajectories. Analysis of the data using different assumptions will partition population into these two bins differently and may remove this sharp dip, but the general shape of the DCS will remain unchanged, being predominantly backward with some sideward and forward scattering.

3. Reagent alignment effects

The effect of HD reagent alignment on the reaction was studied using SRP to prepare highly aligned HD($v=1, J=2$) via the $S(0)$ transition. The polarizations of the SRP pump and Stokes lasers were parallel to each other, and ion arrival profiles were recorded with the SRP polarizations parallel and perpendicular to the detection axis. Additionally, the photolysis laser polarization was also alternated during the course of the experiment to lie parallel or perpendicular to the detection axis. Thus, four polarization-dependent ion arrival profiles were recorded for every experiment; these four profiles are shown in Fig. 5 along with a best fit to the data. These experimental geometries are defined relative to a laboratory-frame coordinate system in which the Z axis is the detection axis, the Y axis is the laser propagation direction, and the X axis is defined by $Z \times Y$. The marked dependence of the experimental profiles on SRP laser polarization indicates that reagent alignment effects are significant.

Excitation through the $S(0)$ transition prepares HD($v=1, J=2, M=0$), and this alignment can be described in terms of spherical tensor alignment moments, $a_0^2 = -\sqrt{2/7}$

and an a_0^4 value of 2/7, with respect to the SRP polarization direction. (An a_0^2 of $-\sqrt{2/7}$ equates to an A_0^2 of -1.) The experiment is less sensitive to reagent a_0^4 alignment effects than it is to a_0^2 alignment effects; therefore, this higher-order moment is ignored in the analysis. As was detailed in Sec. III, the effect of this laboratory-frame a_0^2 preparation on reactivity is expressed by three center-of-mass-frame normalized J-PDDCSs, $S_0^{\{2\}}/S_{00}$, $S_{1+}^{\{2\}}/S_{00}$, and $S_{2+}^{\{2\}}/S_{00}$.

The probability density function [Eq. (1)] can be used to extract reagent alignment effects from the data. In order to accomplish this task, this equation must be convoluted with the distribution of HD rotational axes resulting from the SRP preparation. Furthermore, as optical preparation aligns $\mathbf{J_{HD}}$ in the laboratory frame, each reactive collision will have a different $\mathbf{J_{HD}}$ distribution in the $\mathbf{k,k'}$ frame. Thus, the polarization-dependent reactivity will depend on the prepared alignment a_0^2, the values of the DCS (S_{00}) and J-PDDCSs, and the polar and azimuthal angles ρ and χ which relate the $\mathbf{k,k'}$ scattering frame and the laboratory frame. This probability density function is

$$P(\rho,\chi) = S_{00} + 5a_0^2 \left[S_0^{\{2\}} P_2(\cos\rho) + \frac{\sqrt{3}}{2} S_{1+}^{\{2\}} \sin 2\rho \cos\chi \right.$$
$$\left. + \frac{\sqrt{3}}{2} S_{2+}^{\{2\}} \sin^2\rho \cos 2\chi \right]. \quad (3)$$

Each product in the laboratory frame results from a distribution of possible reagent approach directions. Each of these collisions has a different value of ρ and χ and thus a different dependence on the J-PDDCSs. In order to determine the experimental sensitivity to these moments for a given product, reagent alignment effects must be integrated over all possible $\mathbf{v_{Cl}}$ velocities. Additionally, this integral needs to be weighted by the distribution of reagent velocities, which is determined by the photolysis polarization and the anisotropy, β, of the photodissociation. As a Monte Carlo algorithm is used to generate basis functions, this algorithm is easily expanded to perform the relevant integral numerically. In order to fit the data, these polarization-dependent basis functions were generated for each reagent alignment moment and each experimental geometry.

The analysis method previously used in this laboratory to obtain alignment moments for reagent steric effects[18] and product rotational alignment[37,38] is not ideally suited to the current study. In previous analyses, the data was fit separately to obtain the DCS and the alignment moments. The DCS was fit by summing experimental profiles to yield a composite isotropic profile, $I_\parallel + 2I_\perp$. Then, alignment moments were extracted from anisotropic profiles, $2(I_\parallel - I_\perp)$, from one or more experimental geometries. This methodology is not optimal for the analysis of Cl+HD reagent alignment for two reasons. First, cylindrical symmetry in the experiment is broken by the photolysis laser polarization, and consequently the ''isotropic'' profile contains a dependence on alignment as well; because the alignment effects are very large, this effect becomes significant. Second, as we need to fit four parameters to the data (the DCS and three alignment moments), we require all four experimental geometries, and cannot reduce this number through the formation of composite profiles. Consequently, all four experimental profiles are

fit simultaneously without the formation of composite profiles. We have verified that the three alignment moments produce basis functions which are linearly independent, and thus the parameters obtained are, in theory, uniquely determined. However, the signal-to-noise in this experiment results in some covariance between the polarization moments. For this reason, in hindsight it would have been advantageous to acquire an additional experimental geometry with the photolysis polarization (or the reagent alignment preparation) along the laboratory Y axis (the current SRP and photolysis laser propagation axis.)

We generated 48 basis functions for each of the four polarization geometries. Four basis functions were generated for each product speed to account for the four terms in Eq. (3); 12 product speeds were used to fit the data, as the increased number of speeds (probably exceeding the experimental resolution) insures that the scattering-angle-dependent sensitivity of the alignment moments is correctly modeled. Collision energy and product state distributions were not accounted for in these basis functions. All four experimental geometries were recorded during each experiment, and thus the relative intensities of each profile are well determined experimentally. The four experimental profiles were then fit simultaneously. A least-squares-fitting procedure was used to extract scattering-angle-averaged polarization parameters for HCl($v'=1$) products. A modified maximum-entropy algorithm was also found to be successful in fitting the data (resulting in scattering-angle-dependent J-PDDCSs), and yielded very similar results to the least-squares analysis. The least-squares analysis is used, however, because the variance-covariance matrix facilitates the estimation of statistical error bars.

The resulting fit is shown along with the data in Fig. 5. Polarization parameters obtained for HCl($v'=1$) are $s_0^{\{2\}} = -0.04 \pm 0.27$, $s_{1+}^{\{2\}} = 0.37 \pm 0.14$, and $s_{2+}^{\{2\}} = -0.07 \pm 0.15$. The error estimates are single-parameter variances; that is, they indicate the maximum deviation of a single parameter if the other two values are fixed. Covariances in the data are not overly large and are negative for $s_0^{\{2\}}$ and $s_{1+}^{\{2\}}$ and for $s_{1+}^{\{2\}}$ and $s_{2+}^{\{2\}}$. Thus, acceptable fits to the data are also produced for larger negative values of $s_0^{\{2\}}$ and $s_{2+}^{\{2\}}$, along with smaller values of $s_{1+}^{\{2\}}$. There was insufficient signal to measure alignment effects unambiguously for HCl($v'=0$).

For HCl($v'=1$), the reagent alignment moments are significant, especially for the back-scattered product. A physical interpretation of the measured reagent alignment parameters indicates that reaction favors collision geometries where $\mathbf{v_{Cl}}$ and $\mathbf{J_{HD}}$ are perpendicular, and the resulting products have some preference to scatter in the plane perpendicular to $\mathbf{J_{HD}}$. Furthermore, products scatter preferentially when $\mathbf{J_{HD}}$ is tilted ''away'' from $\mathbf{v_{Cl}}$, along the $x+z$ axis. In interpreting the reagent alignment effects, it should be noted that the experiment does not distinguish between alignment effects with respect to $\mathbf{J_{HD}}$ or with respect the H–D bond.

In analyzing reagent alignment, we have ignored the higher-order alignment moments (the $S_q^{\{k\}}$, $k>2$), as well as three- and four-vector correlations resulting from the alignment of the Cl atom. These effects are likely to be small. Simulations indicate that the experiment is less sensitive to
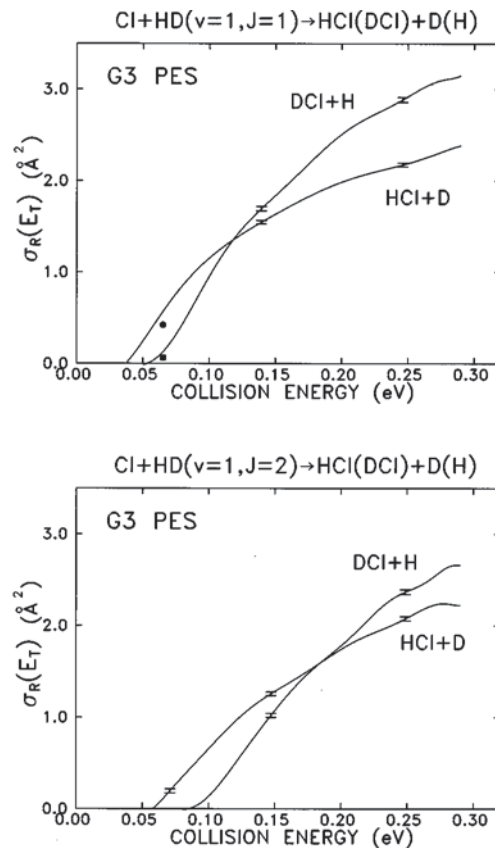

FIG. 6. Solid lines: QCT excitation functions, $\sigma_R(E_{col})$, for the Cl+HD($v=1,J=1$) (top panel) and Cl+HD($v=1,J=2$) (bottom panel) reactions yielding HCl+D and DCl+H products calculated on the G3 PES. Solid symbols: QM reaction cross sections at the fixed collision energy $E_{col} = 0.065$ eV.

the prepared a_0^4. For the Cl-atom alignment effects, only the $\mathbf{a}_2^{(2)}(\perp)$ moment influences the alignment measurements, and hyperfine depolarization reduces its value substantially (-0.09).[39] Therefore, it is unlikely that these additional phenomena will change the total magnitude of the observed alignment. However, as these processes will depend differently on pump and photolysis polarizations, small contributions to the signal could cause the analysis to shift intensity between the $S_0^{\{2\}}$, $S_{1+}^{\{2\}}$, and $S_{2+}^{\{2\}}$. It is also possible that residual thermal motion of the HD reagent will reduce the size of the observed alignment effects, though we estimate the magnitude of this reduction to be relatively small. All of these possibilities should be kept in mind when comparing experimental and theoretical results.

B. Theoretical results

1. Excitation functions and differential cross sections

The lines in the top panel of Fig. 6 correspond to the QCT excitation functions for the two channels of the Cl+HD($v=1,J=1$) reaction calculated on the G3 PES. It is interesting to note that the threshold for the reaction yielding DCl+H is larger than the one for the production of HCl+D. Moreover, the cross sections corresponding to the formation of DCl molecules are smaller than those for HCl production from threshold up to a collision energy of about 0.12 eV, and

from that value the DCl+H channel becomes more reactive than the HCl+D channel. This behavior was observed previously by Persky[40] for the Cl+HD($v=0$) reaction in QCT calculations on the strongly collinear LEPS-type GSW PES, and is in agreement with previous QCT calculations on the G3 PES.[16] In the QCT calculations of Persky, it was found that the isotopic branching ratio $\Gamma = \sigma_R(\text{HCl})/\sigma_R(\text{DCl})$ strongly depends on E_{col} and initial J and, whereas at low collision energy, HCl is the predominant product, as E_{col} increases Γ decreases rapidly, becoming less than unity. The fact that the center of mass of the HD molecule is closer to the D atom implies a greater cone of acceptance for the attack of Cl to this end of the molecule, and thus, the reaction to produce DCl will be more likely. However, given the asymmetry of the PES, the collisions of Cl atoms with the H end of the molecule will take place at larger distances than those with the D end, and the threshold for production of DCl molecules will be larger than the corresponding one for HCl. As can be seen in the lower panel of Fig. 6, HD rotation has an overall negative effect on reactivity, behavior that was previously observed in QCT calculations for the Cl+H$_2$($v=0$) and Cl+D$_2$($v=0$) reactions on the G3 PES.[15] In addition, initial rotation favors the formation of HCl molecules and produces an increase of the threshold for the production of DCl products, in agreement with the results of Persky.[40]

The solid symbols in the top panel of Fig. 6 correspond to the QM reaction cross sections calculated at the fixed collision energy of 0.065 eV. As can be seen, the QM cross sections are slightly smaller than their QCT counterparts, and this fact could indicate that the zero-point energy constraints at the saddle point compensate the tunneling effect for the reaction of Cl atoms with HD molecules in $v=1$.

Figure 7 depicts the QCT vibrationally state-resolved excitation functions for the two channels of the Cl+HD($v=1,J=1$) reaction. For the reaction yielding HCl molecules, the most populated v' state from threshold up to the highest collision energy calculated is $v'=1$. In particular, at $E_{\text{col}}=0.10$ eV, the $v'=1/v'=0$ ratio is about 2 and this ratio increases with collision energy. The most populated DCl vibrational state is also $v'=1$. However, for this channel of the reaction, the QCT calculation predicts a substantial production of DCl molecules in $v'=2$ and a $v'=1/v'=0$ ratio significantly smaller than that for the HCl+D channel. As can be seen, the QM v' state-resolved cross sections at $E_{\text{col}}=0.065$ eV are smaller than the QCT ones (see comments above). At this collision energy, the QCT calculation predicts a cross section of 0.025 Å^2 for the production of DCl($v'=2$), in contrast with the QM results, for which this channel is energetically closed. This result arises from the binning procedure used for the assignment of final rovibrational states in the QCT method in which trajectories with vibrational energy less than that corresponding to $v'=2$ are assigned to this state.

Three-dimensional (3D) perspectives of the collision-energy-dependent DCSs for the reaction yielding HCl($v'=0,1$)+D calculated quasiclassically are shown in Fig. 8. For the HCl($v'=0$)+D channel, the DCSs are markedly backward at the lowest collision energies, and they become more sideways as the collision energy increases. The same
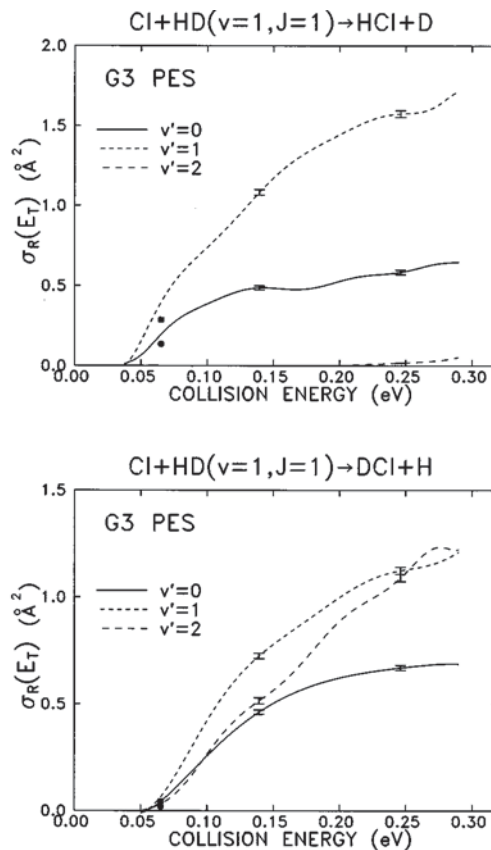

FIG. 7. Lines: QCT vibrationally state-resolved excitation functions for the Cl+HD($v=1,J=1$) reaction. Solid symbols: QM reaction cross sections at the fixed collision energy $E_{\text{col}}=0.065$ eV.

behavior is observed for the HCl($v'=1$)+D channel, but in this case forward scattering starts to appear at collision energies larger than 0.15 eV. At the highest collision energies calculated in this work ($\approx$0.25 eV), forward and sideways scattering becomes more important in the DCSs, in agreement with previous QCT calculations for the title reaction at $E_{\text{col}}=0.2775$ eV.[16] Some of the v' state-resolved DCSs at selected collision energies between 0.05 eV up to 0.25 eV are depicted in Fig. 9. The corresponding DCSs for the reaction yielding DCl($v'=0,1$)+H are also shown. In this case, the DCSs are less sideways and the forward peak smaller than the ones for the HCl($v'=0,1$)+D channel. For both channels, the v' state-resolved DCSs are backward with some sideways component at the collision energies spanned by the experiment.

Figure 10 shows the comparison of the QM and QCT total and v' state-resolved DCSs for both channels of the reaction calculated at the experimental mean collision energy $E_{\text{col}}=0.065$ eV. Apart from the smaller cross section values found in the QM calculations (see comments above), good general agreement between the QM and QCT DCSs is found. Some interesting discrepancies exist; in particular, the QM calculation for the HCl+D channel predicts more sideways scattering and a small peak in the forward direction which is absent in the QCT results. In the case of the DCl+H channel, both QM and QCT DCSs are strongly backward. An important disparity between the QM and QCT results for the pro-

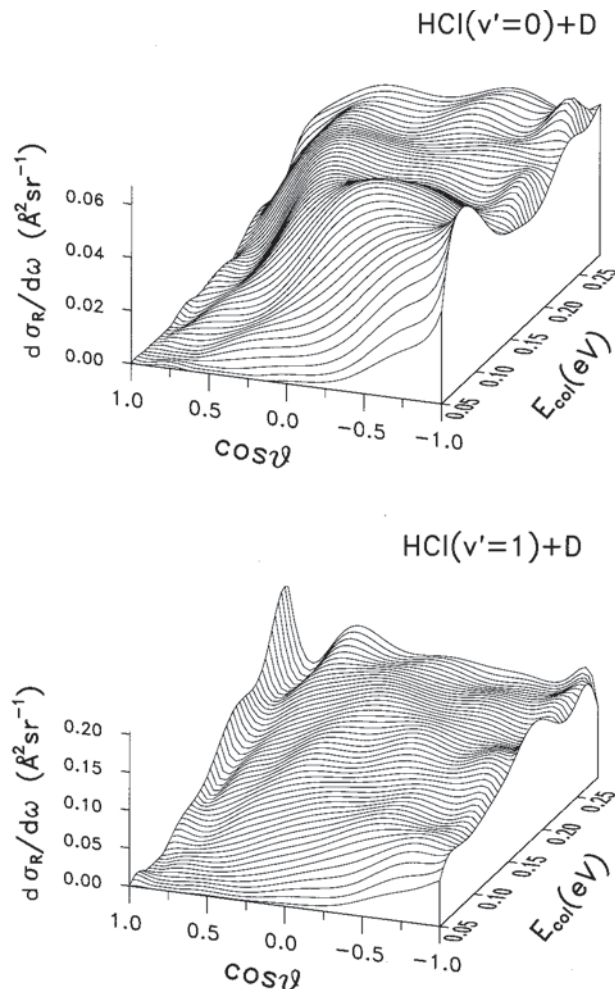FIG. 8. 3D perspective of the collision energy dependent DCSs for the Cl+HD($v=1,J=1$) reaction yielding HCl($v'=0$)+D (top) and HCl($v'=1$)+D (bottom) calculated quasiclassically on the G3 PES. Note the forward peak in the DCSs appearing at collision energies larger than 0.15 eV for the HCl($v'=1$)+D channel of the reaction.

duction of DCl+H is the presence of scattering into DCl($v'=2$) in the QCT case, a channel that is energetically closed at this collision energy in the QM calculation.

The QM and QCT HCl product rotational distributions for $v'=0$ and $v'=1$ calculated at $E_{col}=0.065$ eV are shown in Fig. 11. The QCT rotational distributions are distinctly hotter than the QM distributions, although both theoretical distributions peak at $J'=3$ for HCl($v'=1$). The same tendency has been observed previously for related reactive systems.[1,2] The hotter QCT rotational distributions have been attributed to the binning procedures employed for the assignment of final states (which can assign trajectories with lower vibrational energy to a higher vibrational state).

2. Reagent rotational polarization dependent differential cross sections

Figure 12 depicts the QCT vibrationally state-resolved DCSs and J-PDDCSs for the Cl+HD($v=1,J=2$) →HCl($v'=0,1$)+D reaction calculated at $E_{col}=0.1$ eV on the G3 PES. The calculations have been carried out at $E_{col}=0.1$ eV because the reactivity for $J=2$ is very small at the

experimental mean collision energy of 0.065 eV. As can be seen, the scattering is confined predominantly to the backward hemisphere for both v' states, the DCSs peaking at $\theta \approx 160°$.

The renormalized J-PDDCSs are shown in Fig. 13. Given the low reactivity for θ values below 45°, the large statistical errors prevent the extraction of meaningful information in the forward scattering region.

For both HCl($v'=0$) and HCl($v'=1$) products, the $S_0^{\{2\}}/S_{00}$ moment indicates that $\mathbf{J}$ tends to be polarized with respect to $\mathbf{k}$ at an average value of $\approx 70°$ and does not change with scattering angles. The polarization parameter integrated over scattering angles, $s_0^{\{2\}}$, is -0.271 ± 0.003 and -0.254 ± 0.002 for $v'=0$ and $v'=1$, respectively.

The positive values of the $S_{1+}^{\{2\}}/S_{00}$ moment shown in Fig. 13, indicate a clear tendency for $\mathbf{J}$ alignment to be along the $x+z$ axis. However, the absolute values of the $21+$ moment are relatively small in comparison with the classical limiting values. The polarization parameter $s_{1+}^{\{2\}}$ is 0.144 ± 0.005 and 0.187 ± 0.003 for $v'=0$ and $v'=1$, respectively.

Finally, the value of the $S_{2+}^{\{2\}}/S_{00}$ polarization moment is very small for both v' states, especially in the region where scattering is more important. Only for scattering angles smaller than about 90° does its value become clearly negative, revealing the preference for $\mathbf{J}$ to point along the y axis. The polarization parameter $s_{2+}^{\{2\}}$ is -0.056 ± 0.007 and -0.047 ± 0.004 for $v'=0$ and $v'=1$, respectively, indicating a very small overall tendency of $\mathbf{J}$ to be aligned along the y axis.

For $J=2$, polarization parameters with rank up to 4 can be determined, which includes orientation (odd) and alignment (even) moments. We find that the QCT calculation predicts a very small orientation along the $-y$ axis (the calculated $s_{1-}^{\{1\}}$ is -0.05 and -0.10 for $v'=0$ and $v'=1$, respectively), and the whole distribution can be essentially accounted for by using only the alignment parameters.[40]

C. Comparison between experiment and theory

In this section, the experimental results obtained in the present work for the Cl+HD($v=1,J$) reaction presented in Sec. IV A are compared with the theoretical predictions based on QM and QCT dynamical calculations on the G3 PES presented in Sec. IV B. Note that given the collision energy spread of the experiment, a proper comparison between theory and experiment requires the calculation of collision-energy-averaged theoretical quantities. This averaging is only possible for the QCT calculations which have been performed for the Cl+HD reaction as a function of collision energy (see Sec. III). Given the high computational cost of the QM calculations, they were carried out only at the experimental mean collision energy of 0.065 eV.

Table I shows the experimental and theoretical isotopic branching ratios Γ (DCl/HCl), and the vibrational branching ratios $\Gamma(v'=1/v'=0)$ for the HCl+D channel of the reaction. As can be seen, both theoretical (QCT and QM) calculations predict a clear preference for production of HCl over DCl at the mean collision energy of the experiment
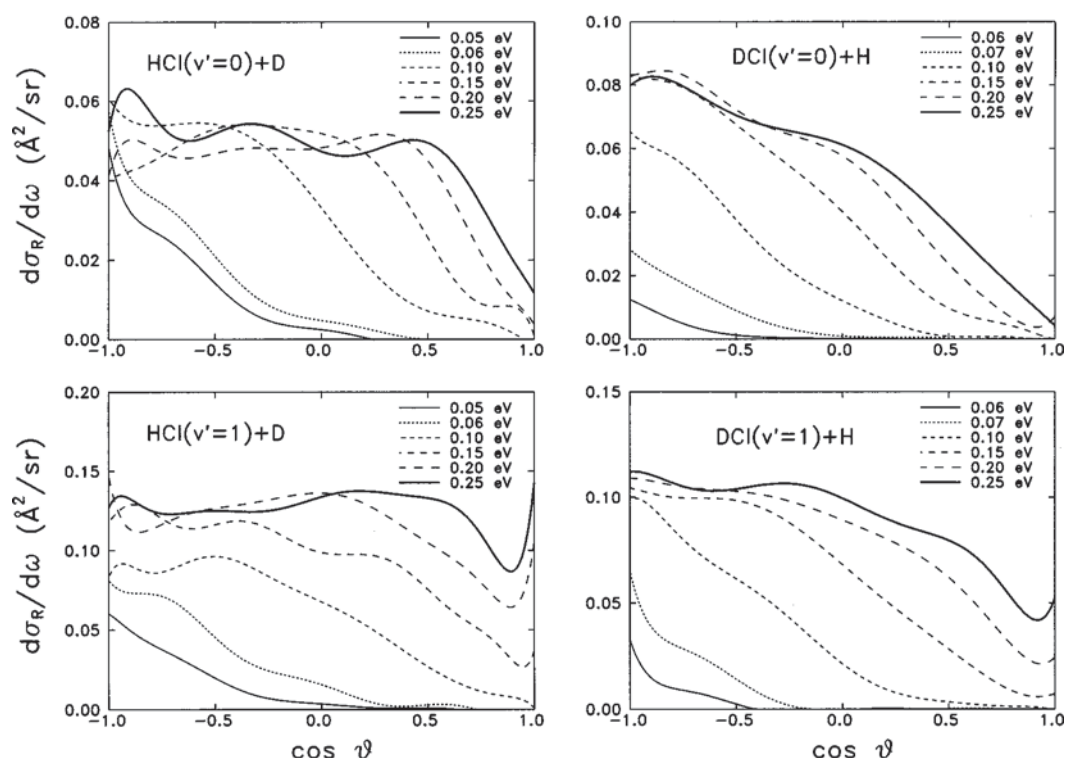
FIG. 9. QCT vibrationally state-resolved DCSs at selected collision energies between 0.05 eV up to 0.25 eV for the two product channels of the Cl+HD($v=1,J=1$) reaction calculated on the G3 PES.

(Γ(DCl/HCl) = 0.18 and 0.15, respectively) in contrast with the measurements, which show a branching ratio close to unity. Once the QCT excitation functions are convoluted with the experimental collision energy distribution, this ratio increases to 0.32, still far from the experimental value. The HCl vibrational branching ratio, $\Gamma(v'=1/v'=0)$ deduced experimentally is significantly larger than the theoretical values (3.5 vs $\approx$2). In this case, averaging of the QCT results
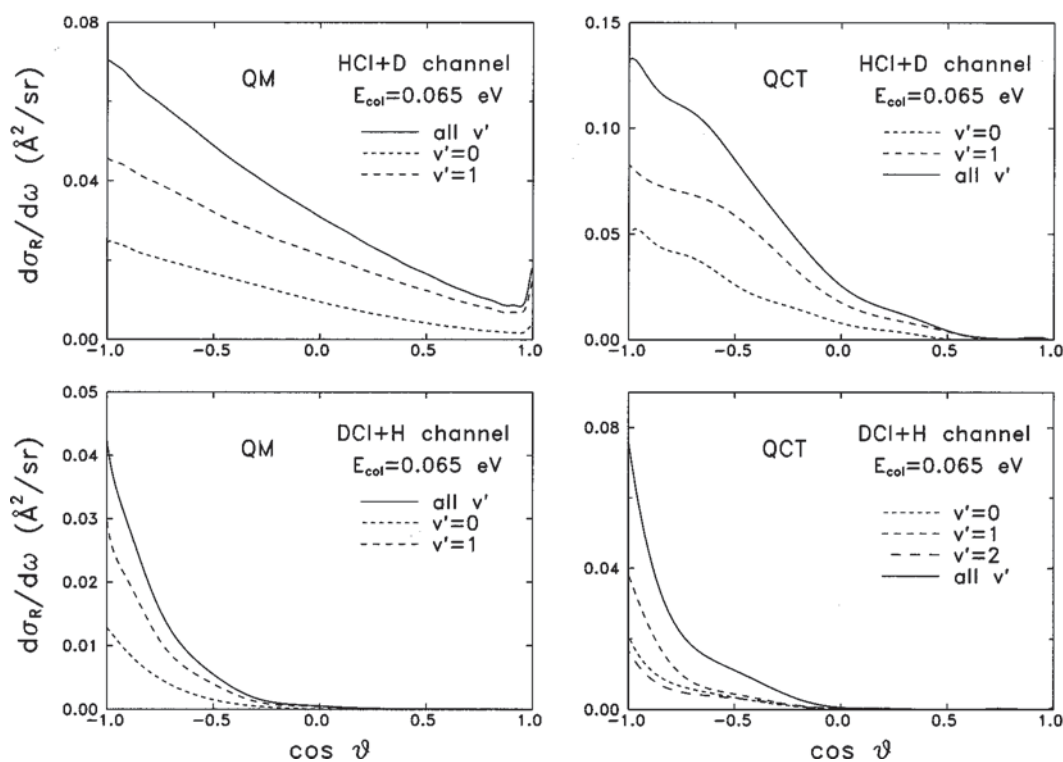
FIG. 10. QM and QCT vibrationally state-resolved DCSs for the Cl+HD($v=1,J=1$) reaction calculated at $E_{col}=0.065$ eV on the G3 PES.
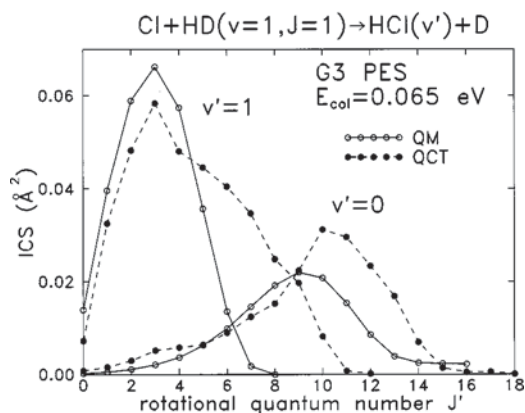
FIG. 11. QM and QCT vibrationally state-resolved product rotational distributions for the Cl+HD(v=1,J=1) reaction yielding HCl molecules calculated at E_{col}=0.065 eV on the G3 PES.

with collision energy does not make a significant difference. These results indicate that the theoretical predictions on the G3 PES are clearly at variance with the experimental data. Given the good agreement found between the QM and QCT results, these discrepancies cannot be attributed to the theoretical methodology. The disagreement between experiment and theory thus indicates either deficiencies in the PES or error in the experimental data (though it should be noted that the measurement of the isotopic branching ratio, in particular, is quite simple and robust.)

The experimental and theoretical product rotational state distributions for HCl(v'=1) are shown in Fig. 14. The theoretical distributions have been scaled to the experimental distribution. Note that the QCT rotational distribution shown

in Fig. 14 has been convoluted with the experimental collision energy distribution, whereas the QM distribution corresponds to the calculation at the fixed collision energy of 0.065 eV. As can be seen, the agreement between the experimental and QM distributions is extremely good. In contrast, the QCT distribution shows somewhat more rotational excitation; this effect, which has been discussed above, is attributed to the binning procedure used in the QCT method. Because the averaged QCT rotational distribution shown in Fig. 14 is very similar to the one obtained from calculations at the fixed collision energy of 0.065 eV (shown in Fig. 11), it is expected that the same applies to the QM case, and thus the good agreement with experiment would remain in the case of a collision-energy-averaged QM rotational distribution.

The experimentally determined DCSs for HCl(v'=0,1) are presented in Fig. 15 along with the collision-energy-averaged QCT DCSs. As can be seen, there is a qualitative agreement between the experimental and QCT data. The experimental DCSs are sideways peaked at about cos θ= -0.4, and this sideways character is larger for v'=1. The QCT DCSs are predominantly backward, although the experimental scattering in the sideways region of the backward hemisphere is well reproduced by the theoretical calculation. The QCT and QM results obtained at the fixed collision energy of 0.065 eV are also predominantly backward (see Fig. 10) and the collision energy evolution of the QCT DCSs shown in Figs. 8 and 9 indicate that the backward character of the DCSs is maintained.

The important issue is to assess whether the observed discrepancies between theory and experiment can be attributed to the assumptions made in the analysis of the experimental profiles, or if they arise from real differences. In par-
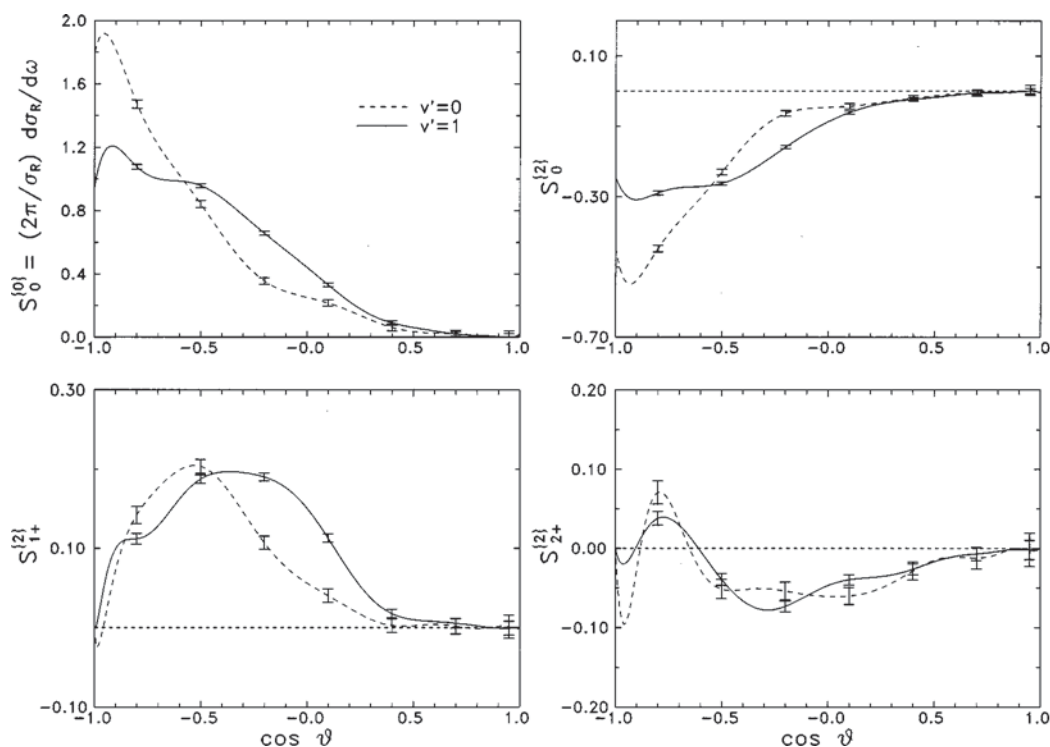

FIG. 12. QCT DCSs and 20, 21+, and 22+ J-PDDCs for the Cl+HD(v=1,J=2) reaction yielding HCl(v'=0,1) molecules calculated at E_{col}=0.10 eV on the G3 PES.

Cl+HD(v=1,j=2)→HCl(v')+D

FIG. 13. QCT renormalized 20, 21+, and 22+ *J*-PDDCSs for the Cl+HD($v=1,J=2$) reaction yielding HCl($v'=0,1$) molecules calculated at $E_{col}=0.10$ eV on the G3 PES.
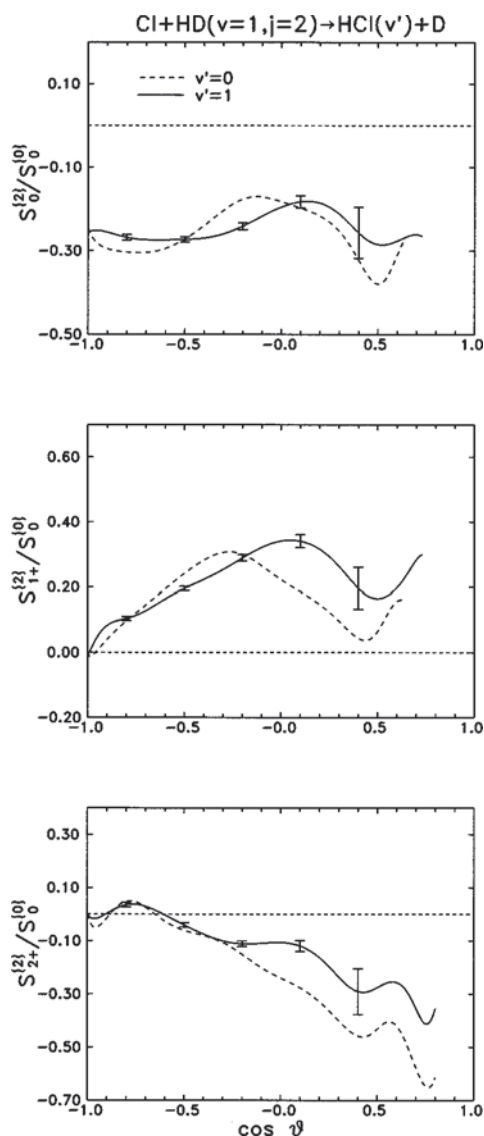
ticular, it is necessary to determine if the peak at $\cos\theta=-0.4$ in the experimental DCS for HCl($v'=1$) and the resulting drop for more backward scattered angles result from the nature of the inversion procedure employed (see discussion in Sec. IV A 2).

TABLE I. Experimental and theoretical isotopic branching ratios Γ(DCl/ HCl) and vibrational branching ratios $\Gamma(v'=1/v'=0)$ for the HCl+D channel. The QCT (averaged) data correspond to the QCT results convoluted with the experimental collision energy distribution, whereas the QCT ($E_{col}=0.065$ eV) and QM ($E_{col}=0.065$ eV) correspond to the QCT and QM calculations carried out at the experimental mean collision energy.

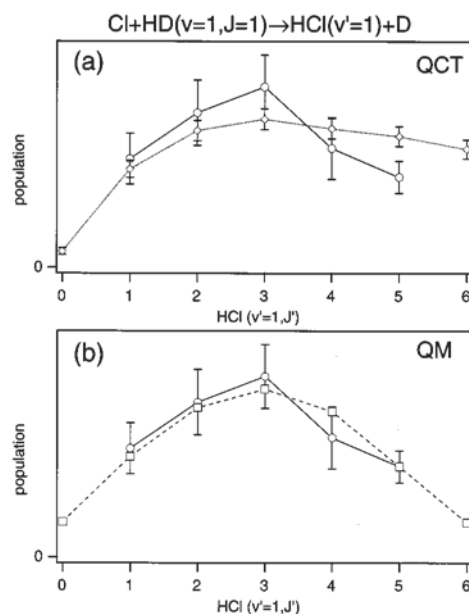|	Γ(DCl/HCl)	$\Gamma(v'=1/v'=0)$
Experiment	0.9 ± 0.2	3.5
QCT (averaged)	0.32	2.00
QCT ($E_{col}=0.065$ eV)	0.18	2.03
QM ($E_{col}=0.065$ eV)	0.15	2.13

Cl+HD(v=1,J=1)→HCl(v'=1)+D

FIG. 14. Comparison of experimental and theoretical rotational state distributions for HCl($v'=1$). Panel (a) shows experimental data (circles, solid lines) and QCT results (diamonds, dotted lines); panel (b) shows experimental data and QM results (squares, dashed lines). Note that agreement is substantially better between the experimental results and the QM theory.

To check this point further, we have forward convoluted the theoretical data, appropriately averaged over product internal states and collision energy, to produce a simulated D-atom arrival profile directly comparable with the one obtained experimentally. The simulated profile is shown in Fig. 16(a) together with the experimental one. This figure shows that the differences between QCT and experimental DCSs are a consequence of true features of the experimental data. The differences between the simulated and experimental D-atom profiles are labeled on the figure and are due to the following: (1) The vibrational branching ratio $\Gamma(v'=1/v'=0)$, which is manifested experimentally by the ratio of slow to fast D atoms, is significantly larger in the measured data than in the QCT simulation (see Table I). (2) The experimental data ''fill in'' more in the center of the profile, which reflects a larger amount of slow D atoms as compared to the QCT simulation; the D atoms with these speeds correspond to sideways- and forward-scattered HCl($v'=1$) molecules, in agreement with the inverted DCSs data. Additionally, it is also observed that the two main peaks in the simulated profile are shifted toward increasing D-atom speeds, thus implying more backward scattering in HCl($v'=1$) than in experiment. Therefore, we conclude that the discrepancies between the experimental and QCT averaged DCSs are real differences.

For H-atom products, a similar forward-convoluted theoretical profile is shown along with the experimental data in Fig. 16(b). These forms are not dissimilar in shape or relative intensities of the central peak and outer ''shoulders,'' indicating that experiment and theory are in rough, qualitative agreement for scattering and vibrational branching of the DCl product. Signal-to-noise considerations, along with the
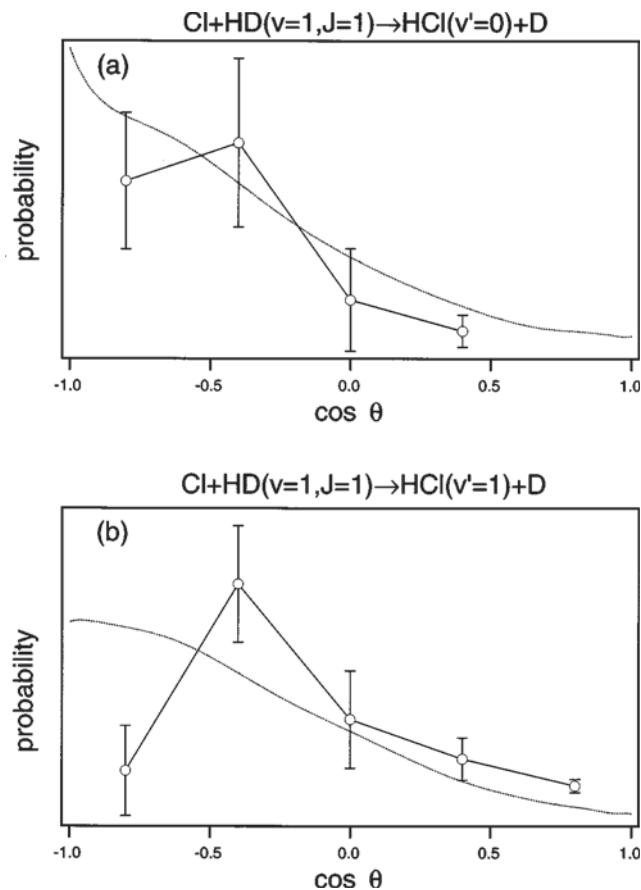
FIG. 15. Comparison of experimental and theoretical differential cross sections for (a) HCl($v'=0$) and (b) HCl($v'=1$) products. The data is shown with error bars for one standard deviation; the theory is from QCT calculations, weighted according to the experimentally determined collision energy distribution.
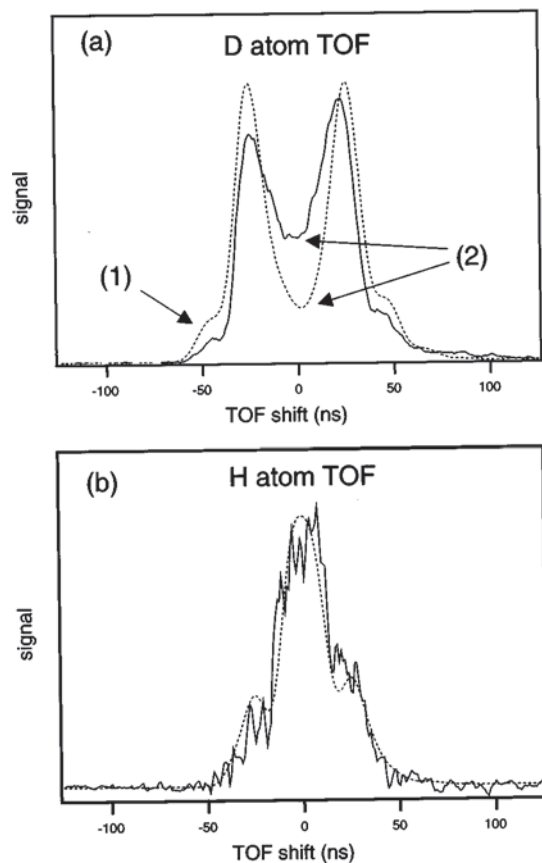
FIG. 16. (a) Experimental D^+ arrival profile (solid line) compared with a forward convoluted simulated profile (dashed line) using the QCT HCl DCSs and vibrational branching ratio. The major deviations between the two profiles are marked and described in the text. (b) Same as (a) but for H^+ arrival profile.

unfavorable kinematics for this channel, prohibit more quantitative comparison.

Experimental measurements are in good agreement with theoretical calculations for the effect of reagent alignment on reactivity, and results are compared in Table II. For HCl($v'=1$) products (which comprise the greatest number of products, for which the most accurate measurement is thus possible), the experimental values are -0.04, 0.37, and -0.07 for the $s_0^{\{2\}}$, $s_{1+}^{\{2\}}$, and $s_{2+}^{\{2\}}$, respectively. The theoretical values for these polarization parameters are -0.26, 0.19, and -0.05. Agreement between experiment and theory is good but not exact, with the measurement and calculation agreeing on the overall magnitude of the alignment effect, as well as the sign of each parameter. All parameters are within or nearly within error bars. As was discussed previously, the covariances in the determination of the experimental parameters support a larger (more negative) $s_0^{\{2\}}$ in conjunction with a smaller $s_{1+}^{\{2\}}$, which is in excellent agreement with the theoretical result. In fact, simulations of the D^+ ion arrival time profiles at the four different geometries of the laser polarization vectors using the QCT polarization parameters has been found in fair agreement with the experimental data.[41]

Reagent alignment effects result from the geometry dependence of reactivity. Consequently, we would expect the

alignment moments to be particularly sensitive to the shape of the potential surface, especially at or near threshold energies. In studies of product rotational alignment, the QCT results have proved to be in good agreement with experiment[42] and with QM calculations,[35] even for very low J'. The current work is one of the first QCT comparisons performed for the reagent angular momentum polarization. Our results for this benchmark reaction indicate that the study of reagent alignment effects can also produce reasonable agreement between experiment and theory.

QCT calculations of the reagent rotational effects in the Cl+H$_2$(D$_2$)($v=0$) isotopic variants of the reaction on the G3 PES have shown that reagent rotational excitation decreases the reactivity, at least for $J<6$ (Ref. 15) at the collision energy of interest. This effect was explained in terms of the

TABLE II. Experimental and theoretical reagent polarization parameters $s_{q+}^{\{k\}}$ for HCl($v'=1$) products. See text for discussion of error estimates (error bars are single-parameter error estimates showing maximum deviation of one parameter when the other two are fixed) and the comparison of experiment to theory.

	$s_0^{\{2\}}$	$s_{1+}^{\{2\}}$	$s_{2+}^{\{2\}}$
Experiment	-0.04 ± 0.27	0.37 ± 0.14	-0.07 ± 0.15
QCT	-0.254	0.187	-0.047

strong collinear character of the G3 PES, where rotational excitation perturbs trajectories approaching the barrier. For the Cl+HD($v=1,J=1,2$) reaction, the present QCT results on the G3 PES show that the isotopic branching ratio (HC+D)/(DCl+H) increases with J, but rotational excitation has a negative effect on the overall reactivity. Notice that the isotopic branching ratio (HCl+D)/(DCl+H) also changes dramatically with collision energy (see Fig. 6); close to the threshold the branching ratio is greater than unity, whereas at collision energies high enough the DCl+H channel dominates. This behavior is in agreement with recent QCT calculations on an empirical LEPS PES reported by Song and Gislason[43] for the Cl+HD($v=0,1$) reaction, in which both vibrational and rotational excitations favor the HCl+D channel of the reaction. These effects are characteristic of strongly collinear potential surfaces, such as the G3 and the empirical LEPS surfaces. A PES with a broader bending potential allowing glancing trajectories to reach the transition state, would augment the orientation effects, changing the picture completely. In that case, rotational excitation would favor reactivity and, furthermore, for a mass-asymmetric system like the title reaction, rotational excitation would favor the DCl+H channel. Preliminary experiments for the measurement of the excitation functions of the Cl+HD($v=0$) reaction[44] seem to indicate that the DCl+H channel strongly dominates over the HCl+D channel from threshold up to 0.32 eV collision energy. The discrepancies between experiment and calculations on the G3 PES found in the present work together with the recent theory and experiments detailed above suggest that the actual PES for this system would differ significantly from the G3 PES.

V. CONCLUSIONS

The dynamics of the Cl+HD($v=1,J=1,2$) reaction have been studied experimentally and theoretically. Isotopic and vibrational branching ratios, rotational distribution of the HCl($v'=1$) product, and differential cross sections have been extracted from the experimental measurements using the photoloc/core-extraction technique. In addition, the effect of the alignment of the reagent angular momentum polarization on reactivity has been investigated for the Cl+HD($v=1,J=2$) reaction. Experimental results have been compared with quasiclassical and quantum mechanical dynamical calculations that have been carried out for the title reaction on the G3 potential energy surface.

Experimental and calculated isotopic and vibrational branching ratios show substantial differences. The collision-energy-averaged QCT calculated value for Γ(DCl/HCl) is 0.32, compared to the experimental measurement of 0.9 $\pm$ 0.2. Averaging over collision energy was not possible for the QM calculations, but as QM and QCT yield similar results at 0.065 eV, the experimental value is also not expected to be in agreement with QM calculations. Experimental measurement of the HCl vibrational branching ratio, $\Gamma(v'=1,v'=0)$, yields a value of 3.5, as compared to QCT and QM calculated values of approximately 2. In contrast, the experimentally determined HCl($v'=1$) rotational state distribution is in extremely good agreement with the QM cal-

culation. The rotational state distribution from QCT calculations is qualitatively similar, but it does not agree with experiment nearly as well as the QM result.

Experimental DCSs for HCl($v'=0$) and HCl($v'=1$) are both backward- and side-scattered, with very little forward scattering evident. This result agrees quantitatively with collision-energy-averaged QCT calculations. Small differences between the experimental and theoretical cross sections are observed, including a greater preference for sideways scattering that is seen in the experimental data. These differences are borne out in a direct comparison of the experimental D$^+$ arrival profile with a theoretical profile that is forward convoluted from the QCT calculations.

The effect of HD rotational alignment on reactivity was determined experimentally and theoretically. Experimental measurement shows that HD rotational alignment has a significant effect on the Cl+HD($v=1,J=2$) reaction, with product formation taking place preferentially when Cl approaches perpendicular to $\mathbf{J_{HD}}$; that is, in the classical plane of rotation of the HD reagent. Furthermore, HCl products tend to scatter in the same plane with a propensity to scatter along the xz plane. QCT-calculated reagent alignment moments are in good agreement, showing the same sign and magnitude as the experimental results.

This work embodies an extensive comparison between experimental measurement and QCT and QM calculations for the Cl+HD ($v=1$; $J=1,2$) reaction. It is particularly interesting that this comparison includes both marked dissimilarities, such as those observed for product isotopic and vibrational branching ratios, as well as close correspondences between experiment and theory for product state distributions and differential cross sections. This range of behavior provides a rigorous test of the features of the G3 surface. Additionally, the measurement and calculation of reagent alignment effects gives insight into the geometry and dynamics of the reaction, promising a sensitive test for refining the reactive PES.

Recent *ab initio* calculations have permitted the determination of a new global PES for this system,[19] after the majority of calculations were completed using the G3 PES. Although the barrier of the PES is similar to that of the G3 PES, both surfaces show notably different topologies. QM calculations performed for the Cl+HD($v=0$) reaction on this new PES show interesting dynamical differences in comparison with the results obtained on the G3 PES.[45] In particular, these new calculations predict that the DCl channel is more favored than the HCl one, in contrast with the findings on the G3 PES and in agreement with the present experimental results. Moreover, these results seem to account very well for the most recent experimental determination of the excitation functions for the Cl+HD($v=0$) reaction.[44,45] It will be of utmost interest to see whether future calculations on the new PES show closer correspondence to our experimental results.

One important conclusion of the present work is the convenience, if not the necessity, of a close interplay between theoretical and experimental work in order to gain the deepest understanding of the dynamics of chemical reactions. Nowadays, state-of-the-art experiments are able to provide

the most stringent test for accurate theoretical calculations on precise PESs for simple reactive systems. Conversely, an insightful interpretation of the experiments requires sound theoretical calculations of the corresponding dynamical observables experimentally accessible.

ACKNOWLEDGMENTS

[1] F. J. Aoiz, L. Bañares, and V. J. Herrero, in *Advances in Classical Trajectory Methods Vol. III: Comparison of Classical and Quantum Dynamics*, edited by W. L. Hase, (JAI, Connecticut, 1998).

[2] F. J. Aoiz, L. Bañares, and V. J. Herrero, J. Chem. Soc., Faraday Trans. **94**, 2483 (1998).

[3] H. Eyring and M. Polanyi, Z. Phys. Chem. Abt. B **12**, 279 (1931).

[4] J. O. Hirschfelder, H. Eyring, and B. Topley, J. Chem. Phys. **4**, 170 (1936); B. Topley and H. Eyring, *ibid.* **4**, 178 (1936).

[5] A. Wheeler and S. Sato, J. Chem. Phys. **23**, 2465 (1955); K. J. Laidler, *Chemical Kinetics*, 3rd Ed., (Harper and Row, New York, 1987), pp. 14, 288–298.

[6] S. S. Kumaran, K. P. Lim, and J. V. Michael, J. Chem. Phys. **101**, 9487 (1994).

[7] M. Alagia, N. Balucani, P. Casavecchia, D. Stranges, and G. G. Volpi, J. Chem. Soc., Faraday Trans. **91**, 575 (1995).

[8] M. Alagia *et al.*, Science **273**, 1519 (1996).

[9] S. H. Lee, L. H. Lai, K. P. Liu, and H. Chang, J. Chem. Phys. **110**, 8229 (1999); S. H. Lee and K. Liu, *ibid.* **111**, 6253 (1999).

[10] C. A. Parr and D. G. Truhlar, J. Phys. Chem. **75**, 1844 (1971).

[11] M. J. Stern, A. Persky, and F. S. Klein, J. Chem. Phys. **58**, 5697 (1973).

[12] D. W. Schwenke *et al.*, J. Chem. Phys. **90**, 3110 (1989).

[13] T. C. Allison, G. C. Lynch, D. G. Truhlar, and M. S. Gordon, J. Phys. Chem. **100**, 13575 (1996).

[14] S. L. Mielke, T. C. Allison, D. G. Truhlar, and D. W. Schwenke, J. Phys. Chem. **100**, 13588 (1996).

[15] F. J. Aoiz and L. Bañares, J. Phys. Chem. **100**, 18108 (1996).

[16] F. J. Aoiz and L. Bañares, Chem. Phys. Lett. **247**, 232 (1995).

[17] W. R. Simpson *et al.*, J. Chem. Phys. **103**, 7299 (1995).

[18] W. R. Simpson *et al.*, J. Chem. Phys. **103**, 7313 (1995).

[19] W. Bian and H.-J. Werner, J. Chem. Phys. **112**, 220 (2000).

[20] D. S. Green, G. A. Bickel, and S. C. Wallace, J. Mol. Spectrosc. **150**, 388 (1991).

[21] F. J. Aoiz, M. Brouard, P. A. Enriquez, and R. Sayós, J. Chem. Soc., Faraday Trans. **89**, 1427 (1993).

[22] N. E. Shafer, A. J. Orr-Ewing, W. R. Simpson, H. Xu, and R. N. Zare, Chin. Phys. **212**, 155 (1993).

[23] K. Ravichandran, R. Williams, and T. R. Fletcher, Chem. Phys. Lett. **217**, 375 (1994).

[24] D. V. Lanzisera and J. J. Valentini, J. Chem. Phys. **103**, 607 (1995).

[25] G. O. Sitz and R. L. Farrow, J. Chem. Phys. **101**, 4682 (1994).

[26] Y. Matsumi, K. Tonokura, and M. Kawasaki, J. Chem. Phys. **97**, 1065 (1992).

[27] K. P. Huber and G. Herzberg, *Molecular Spectra and Molecular Structure. IV. Constants of Diatomic Molecules* (Van Nostrand–Reinhold, New York, 1979).

[28] W. J. van der Zande *et al.*, J. Phys. Chem. **95**, 8205 (1991).

[29] J. F. Castillo, D. E. Manolopoulos, K. Stark, and H.-J. Werner, J. Chem. Phys. **104**, 6531 (1996).

[30] J. F. Castillo *et al.*, J. Chem. Phys. **109**, 7224 (1998).

[31] F. J. Aoiz *et al.*, J. Phys. Chem. **100**, 4071 (1996).

[32] F. J. Aoiz *et al.*, J. Phys. Chem. A **101**, 6165 (1997).

[33] F. J. Aoiz, V. J. Herrero, and V. Sáez Rábanos, J. Chem. Phys. **97**, 7423 (1992).

[34] F. J. Aoiz, M. Brouard, and P. A. Enriquez, J. Chem. Phys. **105**, 4964 (1996).

[35] M. P. de Miranda, F. J. Aoiz, L. Bañares, and V. Sáez Rábanos, J. Chem. Phys. **111**, 5368 (1999).

[36] N. E. Shafer-Ray, A. J. Orr-Ewing, and R. N. Zare, J. Phys. Chem. **99**, 7591 (1995).

[37] A. J. Orr-Ewing *et al.*, J. Chem. Phys. **106**, 5961 (1997).

[38] T. P. Rakitzis, S. A. Kandel, T. Lev-On, and R. N. Zare, J. Chem. Phys. **107**, 9392 (1997).

[39] T. P. Rakitzis, S. A. Kandel, A. J. Alexander, Z. H. Kim, and R. N. Zare, J. Chem. Phys. **110**, 3351 (1999).

[40] A. Persky, J. Chem. Phys. **70**, 3910 (1979).

[41] A. J. Alexander *et al.*, Faraday Discuss. **113**, 333 (1999).

[42] A. J. Alexander *et al.*, J. Phys. Chem. A **101**, 7544 (1997).

[43] J.-B. Song and E. A. Gislason, Chem. Phys. **237**, 159 (1998).

[44] K. Liu (private communication).

[45] D. Skouteris *et al.*, Science (in press).